Journal of Thermal Engineering, Vol. 7, No. 8, Special Issue 14, pp. xx-xx, December, 2021
Yildiz Technical University Press, Istanbul, Turkey

PERFORMANCE ASSESSMENT OF AN ELECTROLYTE-SUPPORTED AND ANODE-SUPPORTED PLANAR SOLID OXIDE FUEL CELLS HYBRID SYSTEM

Abdulrazzak Akroot[1,*], Lutfu Namlı[2]

ABSTRACT

In this study, a system-level zero-dimensional model for planar solid oxide fuel cell- gas turbine (SOFC/GT) hybrid system has been studied to investigate the effect of diverse operating conditions such as operating pressure, air utilization factor (U_a), and fuel utilization factor (U_f) on the performance of a selected hybrid system. Moreover, the system's power production and performance were discussed in two various configurations: anode-supported model (ASM) and electrolyte-supported model (ESM). This study's models were implemented in Matlab® to calculate the optimum operating parameters and determine the hybrid system's performance characteristics. According to the finding, a maximum of 717.8 kW power is produced at 7.7 bar pressure for the ASM. In contrast, a maximum of 630.3 kW power is produced at 12 bar pressure for ESM. The highest electrical system efficiencies for the ASM and the ESM are 62.32% and 56.23%, respectively.

Keywords: *Electrolyte-Supported Model (ESM), Planar Solid Oxide Fuel Cell (SOFC), Anode-Supported Model (ASM), Energy Analysis, Exergy Analysis.*

INTRODUCTION

Solid oxide fuel cell (SOFC) is a new renewable energy source considered one of the most attractive energy conversion systems that directly convert chemical energy in fuels into electricity and heat. It has the clear advantages of high efficiency, low environmental impact, and more flexibility in fuel choice, which plays a significant role in relieving current and future energy demand, and environmental topics. SOFCs have high working temperatures, which allow them to couple with other thermodynamic cycles, such as a gas turbine (GT), to ensure even higher efficiency. Hybrid systems of SOFC/GT present the best power generation efficiencies in the 75–80% range [1,2].

The SOFCs are classified into three models; cathode -supported, anode-supported, and electrolyte-supported. The nomenclature convention is commonly based on the thickest layer of the cell and works as the mechanical supporting base for the rest of the SOFC elements. The electrolyte is very thin for the anode-supported model, which dramatically decreases the electrolyte ohmic loss. Thus, the ASM can be worked at an intermediate temperature. A high operating temperature is wanted for the electrolyte-supported cell to minimize the ohmic loss of the electrolyte. The high operating temperature leads to decreased fuel cell lifetime and raises manufacturing costs ([3,4].

Several investigators have carried out studies on the hybrid integration of SOFC/GT systems [5,6]. Oryshchyn et al. [7] discussed the impact of fuel utilization on SOFS/GT's power plant and the optimum work output split. The authors showed that the Lower fuel utilization ratio raised the Nernst potential and turbine 'inlet temperature (TIT), while SOFC size dropped. Araki et al.[8]introduced two stages of high and low-temperature planar SOFCs placed in series. They presented that the total thermal efficiency of integrated SOFC/GT reached 56%, and the thermal efficiency of SOFCs was 50.2%.Singh and Singh [9] developed a hybrid model of SOFC/GT. Pre-reformer is used before the SOFC stack to convert the natural gas to hydrogen to enhance the performance of fuel cells. Suther et al. [10] presented a SOFC/GT thermodynamic cycle to study the operating parameter's impact on a suggested hybrid model's performance. The results revealed that the operating temperature and operating pressure enhance system efficiency. Pierobon and Rokni[11] analyzed an Integrated gasification SOFC power plant with a Kalina Cycle fueled by woodchips. Huang and Turan[12] studied the impact of various fuel parameters within the allowable operating ranges on several SOFC/GT hybrid system performances.Kuchonthara et al.[13]developed a SOFC/GT system with heat recovery. The authors investigated the influence of steam recovery on the performance

This paper was recommended for publication in revised form by Regional Editor Mohsen Sheikholeslami
[1]Department of Mechanical Engineering, Karabuk University, Karabuk, Turkey
[2]Department of Mechanical Engineering, Ondokuz Mayis University, Samsun, Turkey
**E-mail address: abdulrazzakakroot@karabuk.edu.tr*
Orcid id: 0000-0002-1561-7260, 0000-0001-9758-0889
Manuscript Received 7 July 2020, Accepted 11 February 2021

of the suggested method. Palsson et al. [14] advanced a steady-state 2-D model of electrolyte-supported SOFC combined with a GT to study various system parameters on the system performance. They presented that system efficiency increases when cell voltage and flow rates of air and fuel are reduced. Jia et al. [15] introduced and compared three different configurations of SOFC systems. The results revealed that the (SOFC-GT-ST) system configuration is more complicated and expansive. Still, its electrical efficiency is close to that of the SOFC/GT configuration. Sarmah and Gogoi[16] studied and compared the performance of three different (SOFC/GT) systems.The authors proved that the hybrid cycle with a single pressure steam turbine model presented better performance and recommended using it. Chitsazet al.[17] introduced a thermodynamic model of SOFC/GT system with gas recycling at cathode and anode for the SOFC. The results revealed that the thermal efficiency with anode gas recycling reaches 82.5%, which is 6% greater than that of the simple proposed system. Sghaier et al. [18] investigated the effect of the ambient temperature and the humidity on the SOFC/GT power system's overall efficiencies. The results presented that the increased ambient temperature and the humidity reduced the system's thermal efficiency. The results revealed that the hybrid system's power decreases when the S/C ratio and rotational speed increase. Saebea et al.[19] enhanced the energy management of a power SOFC/GT system by using cathode and anode recycling gas. They proved that the electrodes' recycling directly impacts the TIT, leading to increased GT performance. Haseli et al. [20] introduced a simulation of a combined GT/SOFC model to study the impact of some input parameters such as SOFC operating pressure and TIT on the system's energy efficiency and irreversibility. Amati et al.[21] presented a comparison and simulation of two various arrangements of a hybrid SOFC coupled with a GT on an exergy basis. The system is fueled by methane, and heat recovery is applied both in the GT and between the topping cycle of SOFC/GT and ST's bottoming cycle. Keshvarparast et al. [22] simulated and analyzed a hybrid power plant of solar-geothermal using Aspen HYSYS 9.0. Ezoji et al. [23] studied the heat recovery of homogeneous charge compression ignition engine, and the results showed the thermal performance enhanced to 27.94%. Abbasi et al [24] presented the integration of a SOFC with the biomass gasification process to determine the optimum system design and investigate its performance.

The comparison between anode and electrolyte SOFC hybrid systems has not been discussed before in previous works. This research addresses this gap by introducing a SOFC/GT hybrid system for two different mechanical supports. Both ASM and ESM are developed and integrated with a GT in Matlab® to boost the power produced and the SOFC/GT system's efficiency.

SYSTEM DESCRIPTION

The model prepared in this work was made for a steady-state SOFC/GT hybrid system. It consists of two prime parts: the pressurized SOFC stack with internal reforming and the conventional Brayton cycle (BC) model. The BC model comprises all wanted system instruments such as air and fuel compressors, burner, recuperators, mixing chamber, GT, and pump. Figure1 presents the hybrid system of SOFC– GT with state points.

Air enters the air compressor (state point 1) and is compressed to the required cycle pressure (state point 2). The air is then gaining thermal energy in a recuperator 2 to increase its temperature to the SOFC operating temperature and then brought to the cathode inlet of the SOFC stack (state point 7). Meantime, pure methane enters the fuel compressor (state point 3), where it is compressed to the SOFC operating pressure requirement, and then the compressed fuel is supplied from the fuel compressor (FC) to the mixer (state point 4). Liquid water enters the pump (state point 14). It is pressurized to the desired pressure (state point 15) and then preheated in the recuperator 3to convert the liquid water to water vapor. The water vapor is then supplied to the mixture (state point 16). Methane will be mixed with water vapor in the mixer and then brought to the recuperator (state point 17). In recuperator 2, the mixture is first preheated to a temperature equal to the SOFC inlet temperature and then brought to the anode inlet of the SOFC stack (state point 5). The mixture at state 5 consists of methane and steam. The electrochemical reactions occur within the fuel cell stack to produce DC power.

After the stack, the residual fuel (state point 6) and excess air (state point 8) mix and react to raise the exhaust gases temperature (state point 9). The high temperature and pressure exhaust gases are expanded through a gas turbine and produce additional power. Then, the turbine hot exhaust gases (state point 9) flow through three recuperators to preheat the fuel, air, and water.

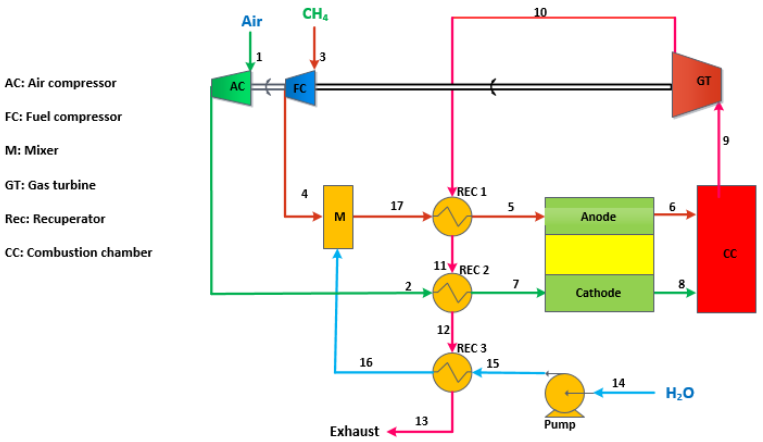

Figure 1. The hybrid system of SOFC – GT with internal reforming

Hybrid Power System Thermodynamic Analysis

Assumption and input data

The mass and energy analysis is accomplished for each device of the hybrid system by using Matlab®. The general assumptions are employed to simplify the simulation are:

- The gas turbine, pump, and compressors are adiabatic.
- Steady-state conditions exist.
- The flow temperature of gases at the inlet and exit of the SOFC stack remains constant.
- No heat losses to the environment.
- The gas mixture at the end of the SOFC stack reaches chemical equilibrium.
- The unreacted gases are fully burned in the burner.

The input data for systems simulation is listed in Table 1.

Table 1. The SOFC Stack Parameters ([25]; [26])

SOFC stack [21] [24]	Cell area, (A_{cell})	$0.01\ (m^2)$
	Exchange current density of the cathode, (i_{oc})	$2500\ (A/m^2)$
	Exchange current density of the anode, (i_{oa})	$6500(A/m^2)$
	Thickness of interconnecting, δ_i	$0.3 * 10^{-2}(m)$
	Baseline current density, (i)	$8000\ (A/m^2)$
	Thickness of cathode, (δ_c)	$50\ (\mu m)$
	Stack pressure drop	2 %
	Fuel utilization factor	$0.85(-)$
	Fuel composition by mass	100% CH_4
	Air composition by mass	21%O_2 79%N_2
	Anode-supported model	
	Thickness of anode, (δ_a)	$500\ (\mu m)$
	Thickness of electrolyte, (δ_e)	$10(\mu m)$
	Electrolyte-supported model	
	Thickness of anode, (δ_c)	$50\ (\mu m)$
	Thickness of electrolyte, (δ_e)	$150(\mu m)$
Recuperator [33]	Pressure drop	3 %

	Effectiveness	80 %
Compressors [33]	Efficiency	85 %
Pump [23]	Efficiency	85 %
Gas turbine [33]	Efficiency	87 %
Afterburner [33]	Pressure drops	5%
	Efficiency	98 %

Thermodynamic Analysis

In this part, the suggested energy system carries out overall mass and energy analyses to give substantial information on system performance and efficiency. The general mass balance and energy balance can be written for all hybrid system components, as illustrated in Table 2.

$$\sum_{\text{in}} \dot{m}_{\text{in}} = \sum_{\text{out}} \dot{m}_{\text{out}} \quad \textbf{(1)}$$

where the subscripts in and out represent inlet and exit, respectively.

$$\dot{Q} + \sum_{\text{in}} \dot{m}_{\text{in}} h_{\text{in}} = \sum_{\text{out}} \dot{m}_{\text{out}} h_{\text{out}} + \dot{W} \quad \textbf{(2)}$$

where $\dot{W}$ is the work transfer rate, and $\dot{Q}$ is the heat transfer rates.

Table 2. The list of mass and energy equations

Components	Mass Balance	Energy Balance
Air Compressor	$\dot{m}_1=\dot{m}_2$	$\dot{m}_1 h_1 + \dot{W}_{AC} = \dot{m}_2 h_2$
Fuel Compressor	$\dot{m}_3=\dot{m}_4$	$\dot{m}_3 h_3 + \dot{W}_{FC} ==\dot{m}_4 h_4$
Mixer	$\dot{m}_4+\dot{m}_{16} = \dot{m}_{17}$	$\dot{m}_4 h_4+\dot{m}_{16} h_{16} = \dot{m}_{17} h_{17}$
Water pump	$\dot{m}_{14}=\dot{m}_{15}$	$\dot{m}_{14} h_{14} + \dot{W}_{WP} = \dot{m}_{15} h_{15}$
Recuperator 1	$\dot{m}_{10} + \dot{m}_{17} = \dot{m}_5 + \dot{m}_{11}$	$\dot{m}_{10} h_{10} + \dot{m}_{17} h_{17} = \dot{m}_5 h_5 + \dot{m}_{11} h_{11}$
Recuperator 1	$\dot{m}_{11} + \dot{m}_2 = \dot{m}_7 + \dot{m}_{12}$	$\dot{m}_{11} h_{11} + \dot{m}_2 h_2 = \dot{m}_7 h_7 + \dot{m}_{12} h_{12}$
Recuperator 1	$\dot{m}_{12} + \dot{m}_{15} = \dot{m}_{13} + \dot{m}_{16}$	$\dot{m}_{12} h_{12} + \dot{m}_{15} h_{15} = \dot{m}_{13} h_{13} + \dot{m}_{17} h_{17}$
Gas turbine	$\dot{m}_9=\dot{m}_{10}$	$\dot{m}_9 h_9 = \dot{m}_{10} h_{10} + \dot{W}_{GT}$
Combustion chamber	$\dot{m}_6+\dot{m}_8 = \dot{m}_9$	$\dot{m}_6 LHV_{fuel}+\dot{m}_8 h_8 = \dot{m}_9 h_9$
SOFC	$\dot{m}_5+\dot{m}_7 = \dot{m}_6 U_f+\dot{m}_6(1-U_f) + \dot{m}_8$	$\dot{m}_7 h_7+\dot{m}_5(U_f) LHV_{fuel} + \dot{m}_5(1-U_f) h_7 = \dot{m}_6(U_f) h_6+\dot{m}_6(1-U_f) h_6+\dot{m}_8 h_8 + W_{SOFC}$

The net power outputs from the integrated system are calculated as:

$$\dot{W}_{\text{Net}} = \dot{W}_{\text{SOFC}} + \dot{W}_{\text{GT}} - \dot{W}_{\text{AC}} - \dot{W}_{\text{FC}} - \dot{W}_{\text{P}} \quad \textbf{(3)}$$

where $\dot{W}_{\text{SOFC}}$ is the SOFC power output, $\dot{W}_{\text{GT}}$ is the GT power output, $\dot{W}_{\text{AC}}$ is the air compressor power input, $\dot{W}_{\text{FC}}$ is the fuel compressor power input, and $\dot{W}_{\text{P}}$ denotes the pump power input.The following equation gives the SOFC power output:

$$\dot{W}_{\text{SOFC}} = i.\,\text{A}_{\text{cell}} \cdot \text{v}_{\text{cell}} \cdot \text{n}_{\text{cell}} \quad \textbf{(4)}$$

where i is the current density in Ampere, $A_{cell}$is the cell area, $v_{cell}$is the cell voltage, $n_{cell}$is the number of cells in the stack. The following equation gives the power output from the fuel cell stack:

$$v_{cell} = E°_{Nernst} - v_{act} - v_{Ohmic} - v_{con} \quad \textbf{(5)}$$

where $E°_{Nernst}$ is the Nernst potential, v_{act} is the activation loss, v_{Ohm} is the ohmic loss, and v_{con} is the concentration loss. The equations needed for calculating voltages are illustrated in Table 3.

Table 3. Electrochemical equations [27,28]

Type	**Equation**
Nernst potential	$E_N = -\frac{\Delta G}{n\,F} + \frac{RT}{2F}\left[\frac{P_{H_2} \cdot P_{O_2}^{1/2}}{P_{H_2O}}\right]$ $\Delta G = -247.4 + 0.0541\,T$
Activation losses	$\eta_{act,a} = \frac{RT_{sofc}}{F}\sinh^{-1}\left(\frac{i}{2i_{oa}}\right)$ $\eta_{act,c} = \frac{RT_{sofc}}{F}\sinh^{-1}\left(\frac{i}{2i_{oc}}\right)$
Ohmic losses	$\eta_{ohm} = i(\rho_a\delta_a + \rho_c\delta_c + \rho_e\delta_e + \rho_i\delta_i)$ $\rho_a = 95 \times 10^6 \exp\left(\frac{-1150}{T_{sofc}}\right)^{-1}$ $\rho_c = 42 \times 10^6 \exp\left(\frac{-1200}{T_{sofc}}\right)^{-1}$ $\rho_e = 3.34 \times 10^4 \exp\left(\frac{-10300}{T_{sofc}}\right)^{-1}$ $\rho_i = 9.3 \times 10^6 \exp\left(\frac{-1100}{T_{sofc}}\right)^{-1}$
Concentration losses	$\eta_{con,a} = \frac{RT_{sofc}}{2F}\left(\ln\left(1 + \frac{P_{H_2} i}{P_{H_2O} i_{as}}\right) - \ln\left(1 - \frac{i}{i_{as}}\right)\right)$ $\eta_{con,c} = -\left(\frac{RT_{sofc}}{2F}\ln\left(1 - \frac{i}{i_{cs}}\right)\right)$ $i_{as} = 2.F.\frac{P_{H_2}.D_{aeff}}{RT_{sofc}L_{an}}$
	$i_{cs} = 4.F.\frac{P_{O_2}.D_{ceff}}{\left(\frac{P_c - P_{O_2}}{P_c}\right)RT_{sofc}L_{an}}$

The electrical efficiency of the integrated system is estimated as:

$$\eta_{th} = \frac{W_{Net}}{m_f LHV_f} \quad \textbf{(6)}$$

where m_f and LHV_fdenote the mass flow rate and the fuel's lower heating, which supplies the integrated system, the electrical exergy efficiency is calculated as:

$$\psi_{electricity} = \frac{W_{Net}}{\dot{n}_f \bar{e}_f^{kim}} \quad \textbf{(7)}$$

where $\bar{e}_f^{kim}$is the standard chemical exergy of the fuel.

RESULTS AND DISCUSSIONS

Validation

The offered hybrid system analysis is advanced, employing a MATLAB program to study the work output and thermal efficiency. The results obtained from the SOFC model were evaluated by comparing the cell voltage with the experimental and numerical results presented in the references [28,32]. Table 4 illustrates the cell voltage reached in this work and the experimental data presented in the literature. The comparison showed compatibility between them, which mentions an agreeable verification of the present model.

Table 4. A comparison of cell voltage was reached in this work with the data from the literature [28,32].

Current density (A/m^2)	Present work	Ranjbar et al. 2014	Tao et al. 2005
0.2	0.76	0.79	0.76
0.3	0.7	0.711	0.68
0.4	0.64	0.644	0.62
0.5	0.57	0.56	0.57
0.6	0.51	0.51	0.52

Figure 2 reveals the influence of operating pressure on cell voltage and stack power. It is clear from this figure that when the SOFC operates at high pressures, the cell voltage v_{cell} increases due to the increase of Nernst potential. When system pressure rises from 4 to 15 bar, cell voltage increases from 0.4911 to 0.5283 V for the ESM, whereas it increases from 0.6765 to 0.7144 V for the anode-supported model. The power created by the SOFCs should be determined from the current density, cell voltage, and the number of cells. Figure 2 also revealed that a rise in the SOFC operating pressure causes an increase in the SOFC power due to the depression in the voltage losses. Figure 2 also showed that a surge in the SOFC operating pressure allows an increase in the stack's overall power due to the depression in the voltage losses. The figure also reveals that when SOFC operating pressure raises from 4 bar to 15 bar, the stack's power boosts from 583.4 to 616.1 kW (about 5.3%) for the ASM. In contrast, the stack's overall power rises from 423.5 to 455.63 kW (about 7%) for the electrolyte-supported model.

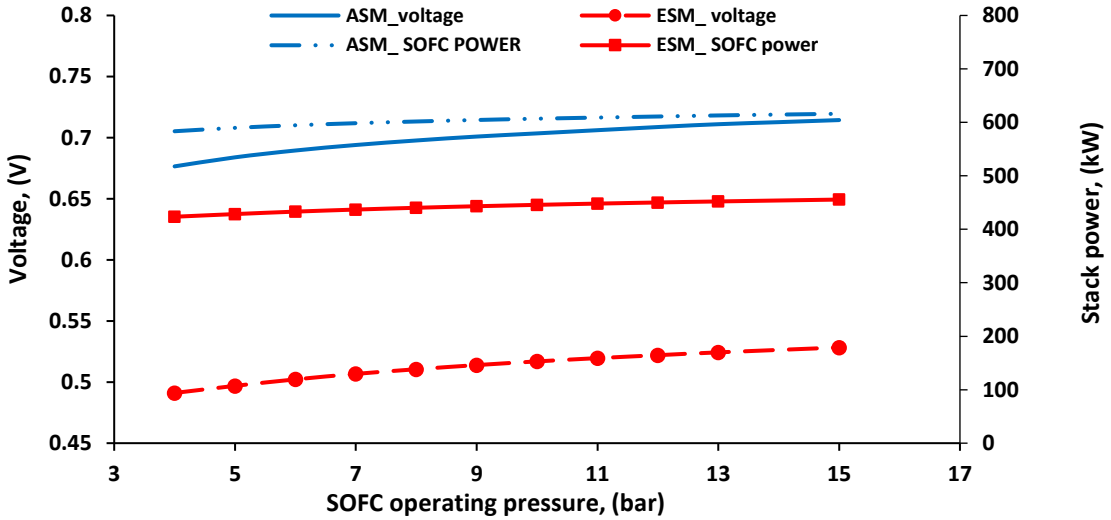

Figure 2. The effect of SOFC operating pressure on the Performance of the fuel cell stack for two various models.

Figure 3 illustrates the impact of the SOFC operating pressure on the GT's net power for two different models. A SOFC- GT hybrid system demands some equipment such as an air compressor, fuel compressor, and pumps that need work input. Consequently, it should deduct the accessory power wasted by these instruments from the total power produced by the GT. It is evident from the figure that the GT net power output boosts with a rise in the operating pressure, attains an ultimate, and then drops as the SOFC operating pressure more increases. The compressor's power considerably increases when the SOFC operating pressure increases too much, diminishing the

GT's net power. The maximal net capacity is 96 kW at 7.7 bar for the ASM, whereas the maximal net capacity is 181.4 kW at 10 bar for the electrolyte-supported model.

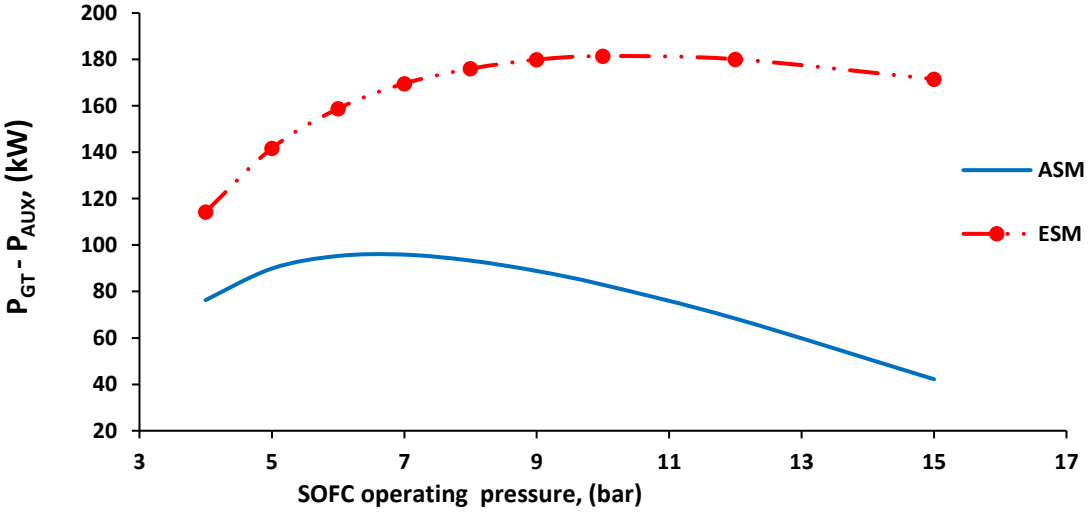

Figure 3. Variation of net power output from the gas turbine with SOFC operating pressure for two various models.

Figure 4 reveals the impact of operating pressure on the total power output for two different models. Increasing the operating pressure causes an increment in the SOFC and GT power output. The results indicated that the total power output raises with rising operating pressure until it amounts to a maximal and then starts to decline as the OFC operating pressure increases. When the SOFC operating pressure rises dramatically, the additional components' power significantly increases, reducing the total power output. The results note that the maximum system's actual power of 695 kW at 7.7 bar for the ASM and a maximum of 630.3 kW at 12 bar for the ESM.

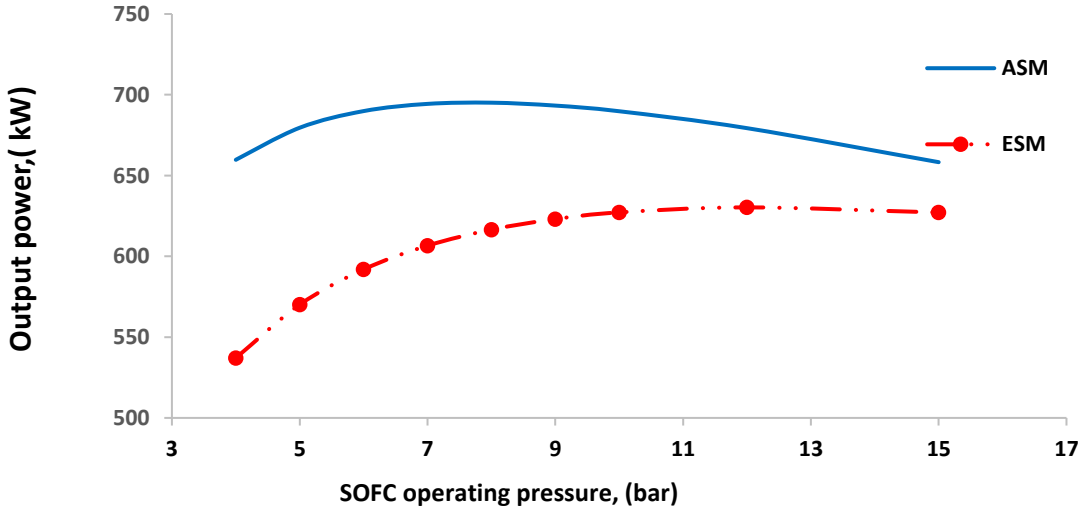

Figure 4. Variation of the overall power output from the hybrid system with SOFC operating pressure for two different models.

Figures 5 and 6 present the relation between the SOFC operating pressure and the system performance for two different models. The fuel cell electrical efficiencies curves represent the relation between the total power generated by SOFC only and the inlet energy or exergy to the system. The stack power and its voltage boost when the SOFC operating pressure increases, enhancing the stack efficiencies. It is presented from the results that when SOFC operating pressure rises from 4 bar to 15 bar, the SOFC efficiency grows from 54.23 to 57.26% for the ASM. In contrast, it increases from 39.3 to 42.4% for the electrolyte-supported model. The SOFC exergy raises from 52.31 to 55.23% for the ASM, whereas it increases from 37.9 to 40.65% for the electrolyte-supported model.

The system efficiencies curves present the relation between the hybrid system's overall power and the system's inlet energy or exergy. The rise of the SOFC operating pressure leads to an increase in the GT inlet pressure, consequently an enhancement in the GT power output and growth in the power-consuming by the auxiliary components. When the SOFC operating pressure raises, the overall efficiencies reach the farthest and then decline as the SOFC operating pressure increases. For a presented system in this research, the electrical efficiency is maximized at a system pressure of 7.7 bar for the ASM. In contrast, the electrical efficiency is maximized at 12 bar for the electrolyte-supported model.

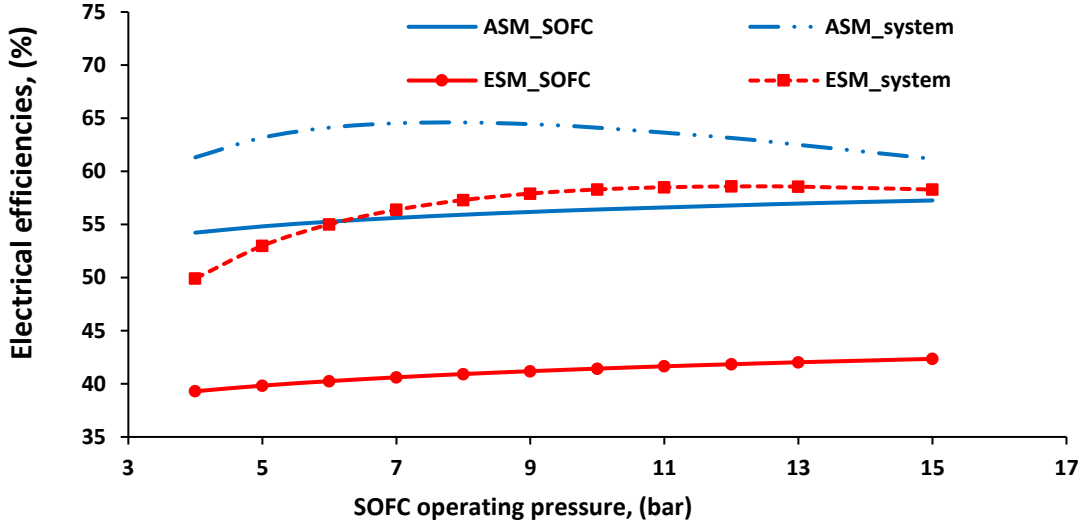

Figure 5.Variation of the electrical efficiencies with SOFC operating pressure for two different models.

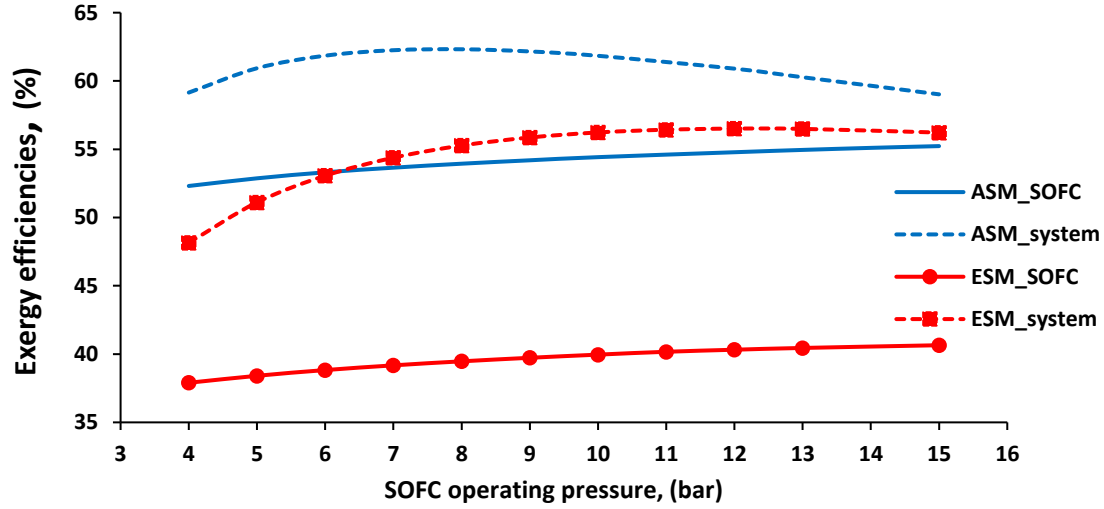

Figure 6.Variation of the exergy efficiencies with SOFC operating pressure for two various models.

The effect of varying fuel utilization factors (Uf) on the hybrid system's performance for two different models is presented in Figures 7–12. fuel utilization factors effect is examined here for a constant SOFC operating pressure and temperature of 7.7 bar and 750 °C for ASM, whereas 10 bar and 1000 °C for the electrolyte-supported model.

Figures 7 and 8 reveal Uf's impact on stack power density, cell voltage, and fuel cell overall power. The curves presented that at a higher value of U_f, the stack power and cell voltage are reduced because of the reduction in the partial pressure of hydrogen at the anode. At lower U_f, the increase in fuel flow rate to the system can convert more chemical energy into electrical power, which means more power density is obtained from the fuel cell. The results also reveal that the cell voltage rises from 0.697 to 0.7457 V for the ASM, whereas it increases from 0.517 to

0.574 V for the ESM when the U_f reduces from 0.85 to 0.65. As shown in Figure 8, decreasing the U_f leads to an increase in the stack power. The reduction in the U_f causes the passing of a large amount of fuel through the GT, raising the specific work generated by the GT and improving the electrical power produced by the system. It is shown from the results that if the U_f reduces from 0.85 to 0.65, the system power elevates from 695.18 to 840.19 kW (about 17.3%) for the ASM, whereas the cell system power elevates from 627.18 to 793.2 kW (about 21%) for the electrolyte-supported model.

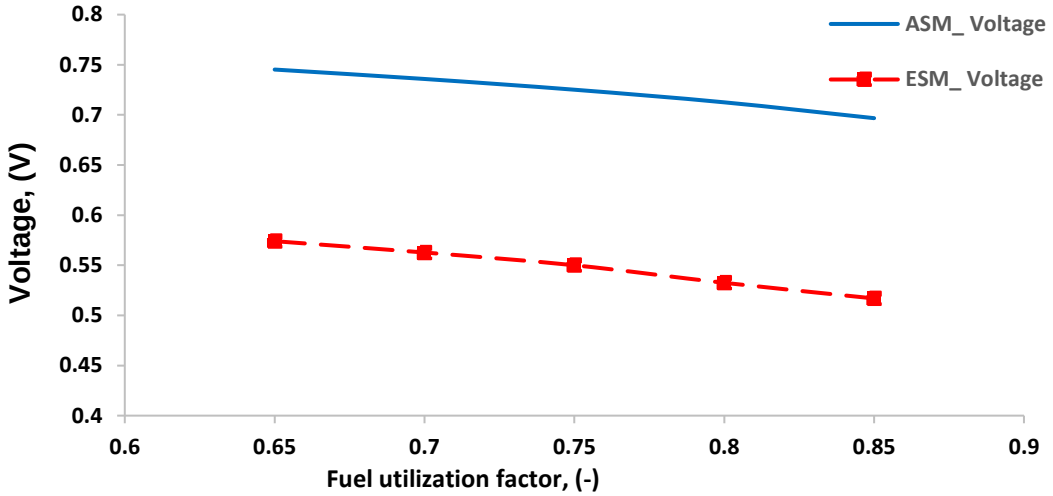

Figure 7. Variation of the cell voltage with the fuel utilization factor for two various models.

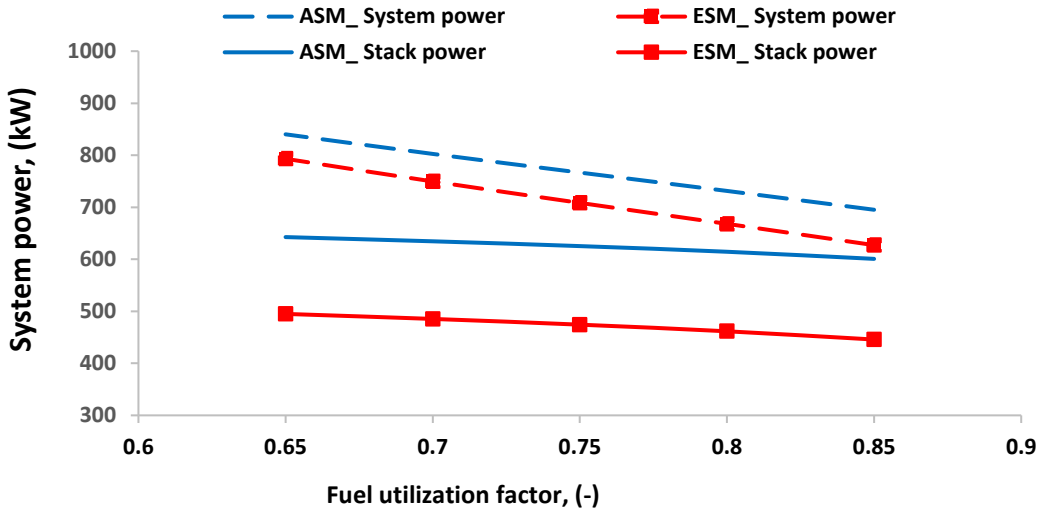

Figure 8. Variation of the hybrid system's total power output with the fuel utilization factor for two different models.

Figure 9 reveals the influence of fuel utilization fac U_f tor on the turbine inlet temperature (TIT) for two different models. The decreased U_f positively impacts the TIT and boosts GT's power, corresponding to the elevated combustion temperature. The figure also showed that the TIT for the ESM is greater than the ASM because the ESM operates at 1000 ° C while the ASM operates at 750 ° C.

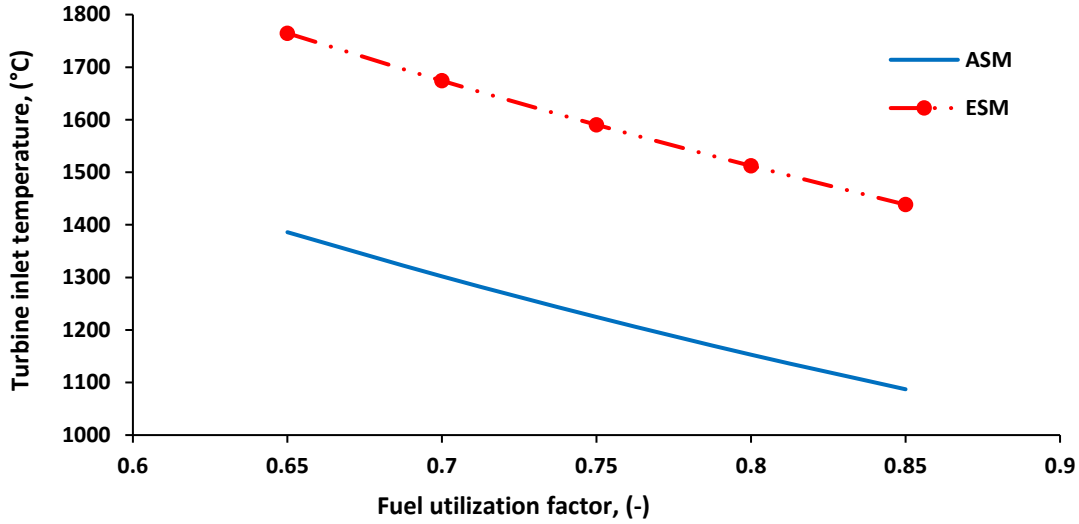

Figure 9. The effect of fuel utilization factor on the turbine inlet temperature (TIT) for two different models.

Figure 10 presents the U_f's influence on the GT's net power for two different models. The power consumption by the compressors is a slight increase with a reduction in the U_f. Still,the gas turbine's produced power increases dramatically, resulting in an increase in the net electrical net power of GT with a lower U_f. It is also presented from figure 10 that the net power of GT elevates from 94.4 to 197.5 kW (about 52.2%) for the ASM, whereas the cell system power promotes from 181.42 to 298.18 kW (about 39.16%) for the ESM when the U_f reduces from 0.85 to 0.65.

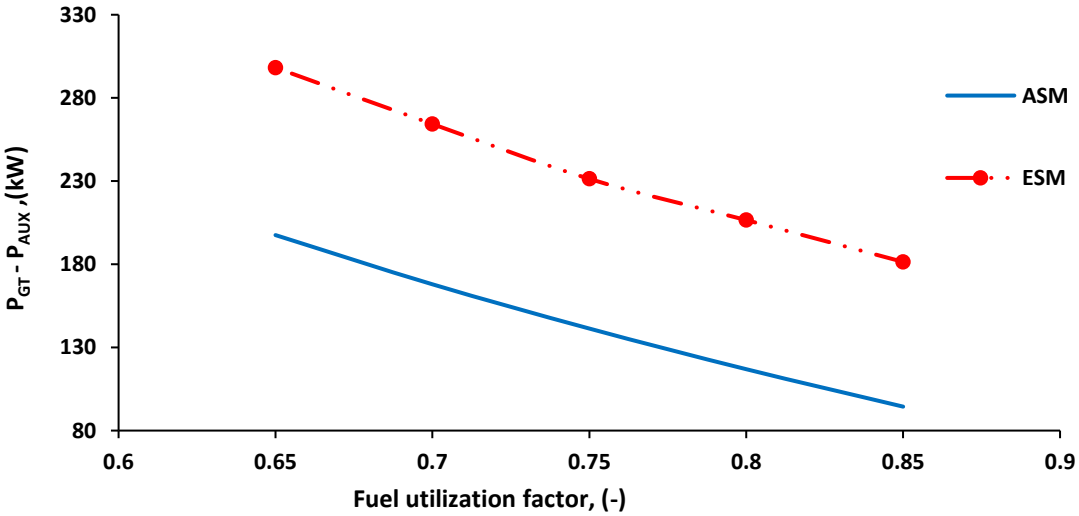

Figure 10. The effect of fuel utilization factor on the GT's net power for two various models.

U_f's impact on the performance of the hybrid system shows in Figure 11 and Figure 12. A reduction in the U_f hurts the hybrid system'senergy efficiencies and exergy efficiencies. The results demonstrated that increasing the U_f reduces the mass flow rate, voltage, and stack power. In contrast, it occurs an improvement in both the electrical efficiency and exergy efficiencies. When the U_f is significantly elevated, virtually all the amount of H_2 created is consumed within the fuel cell by the electrochemical reaction in the anode. It is clear from the results that the SOFC efficiency decreases from 55.84 to 44.7% for the ASM, whereas it reduces from 41.34 to 35.2 % for the electrolyte-supported model. The SOFC exergy decreases from 53.86 to 44.06% for the ASM. In contrast, it reduces from 39.96 to 33.94% for the ESM.

At a high U_f factor, the power produced and system efficiencies are reduced at the same time due to the lower mass flow rate of fuel that enters the hybrid system. Therefore, the increase in the U_f enhances the system thermodynamically and reduces the cost of fuel. It is shown from the results that the overall efficiency reduces from

64.61 to 59.27% for ASM, whereas it reduces from 58.3 to 56.4 % for the ESM. The overall exergy reduces from 53.86 to 44.06% for the ASM. In contrast, it decreases from 39.96 to 33.94% for the ESM.

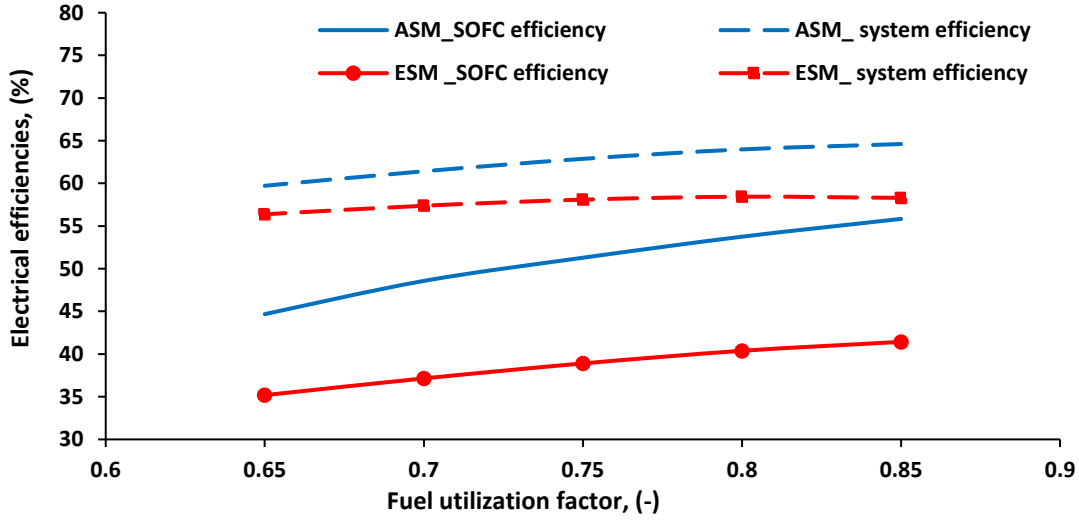

Figure 11. Variation of electrical efficiencies with fuel utilization factor for two various models.

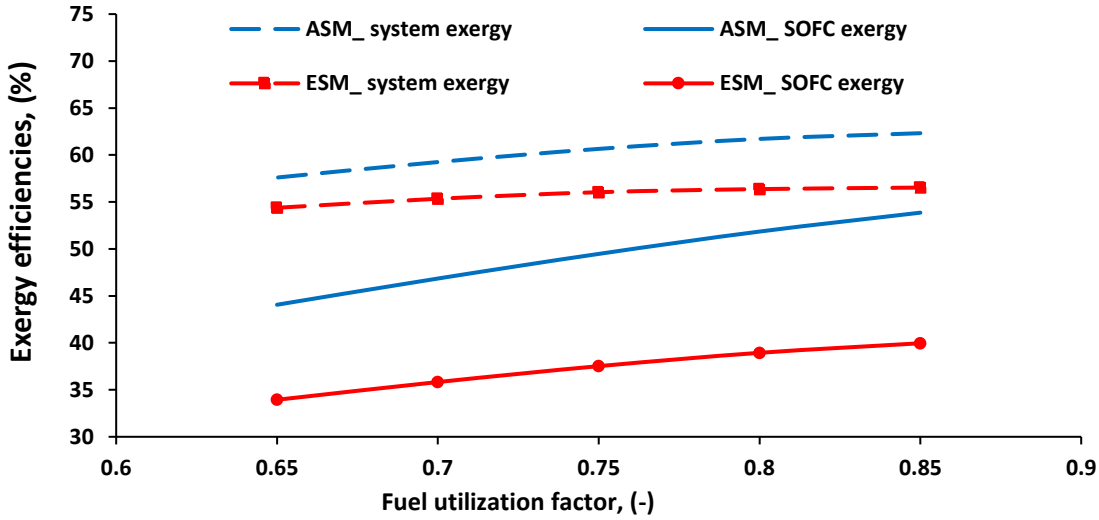

Figure 12. Variation of Exergy efficiencies with fuel utilization factor for two various models.

The air utilization factor (Ua) value is a significant parameter in the hybrid system performance, and it has a cooling impact on the SOFC stack. Figures 13–18indicate the influence of the U_a on the voltage, power output, and system performance for a constant SOFC operating temperature and pressure of 750 °C and 7.7 bar for the ASM, whereas 1000 °C and 10 bar for the ESM.

The U_a's impact on the stack power density, cell voltage, and net electrical power generated by the integrated system is illustrated in Figures 13 and 14. It is worth mentioning that the effect of U_a on stack power density, cell voltage, and overall power output is similar to that of the fuel utilization factor. The results show that the U_a reductionleads to an increment in the stack voltage and the stack power density. It is shown from the results that the cell voltage reduces from 0.6967 to 0.6872 V for the ASM, whereas it reduces from 0.522 to 0.508 V for the ESM. The stack power decreases from 602.6 to 592.7 kW (about 16.4%) for the ASM. In contrast, it falls from 450 to 437 kW (about 29%) for the ESM when the U_a increases from 0.25 to 0.6.

The decrease in the U_a causes passing a higher flow rate of air through the GT, which leads to an increase dramatically in GT power output. Therefore, the total power generated by the system elevates with a reduction in the U_a. It is clear from the results that the system power decreases from 704.6 to 675 kW (about 4.2%) for the ASM, whereas it decreases from 687.3 to 586.6 kW (about 14.6%) for the ESM when the U_a increases from 0.25 to 0.6.

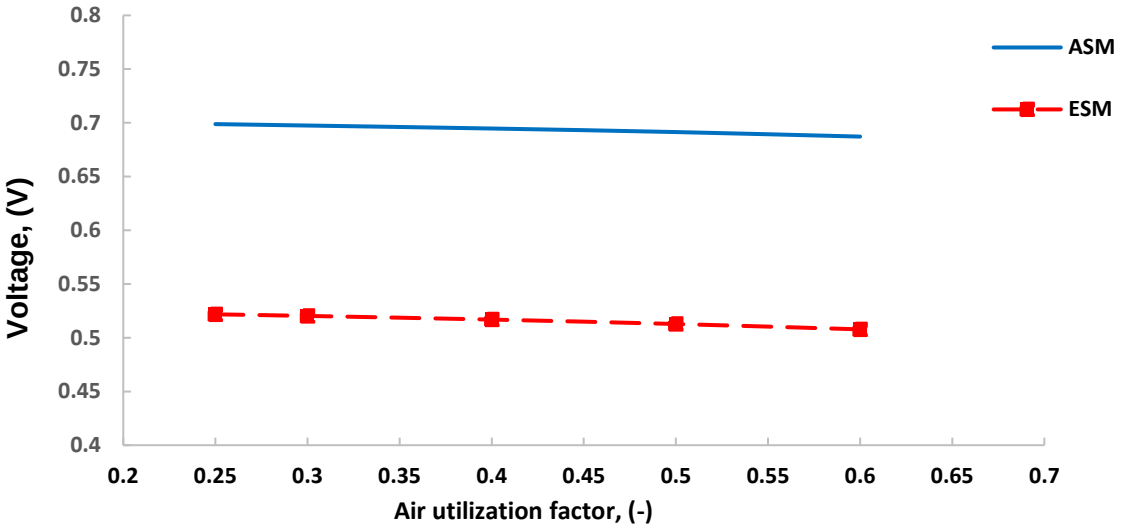

Figure 13. Variation of cell voltage with an air utilization factor for two various models

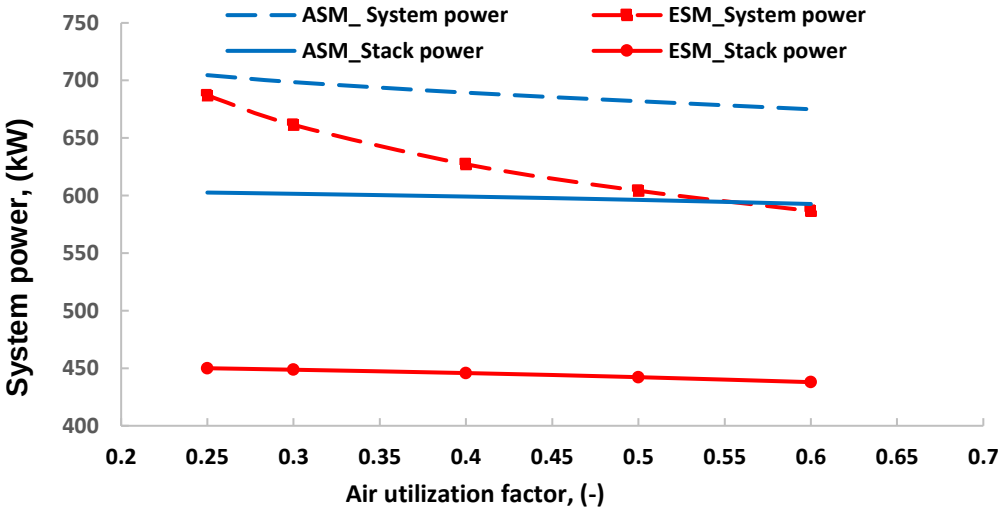

Figure 14. Variation of output power with an air utilization factor for two various models

Figure 15 presents the impact of the U_a on the turbine inlet temperature (TIT). The figure revealed that the TIT increases with an increase in the U_a due to the decrease in air mass flow to the GT.

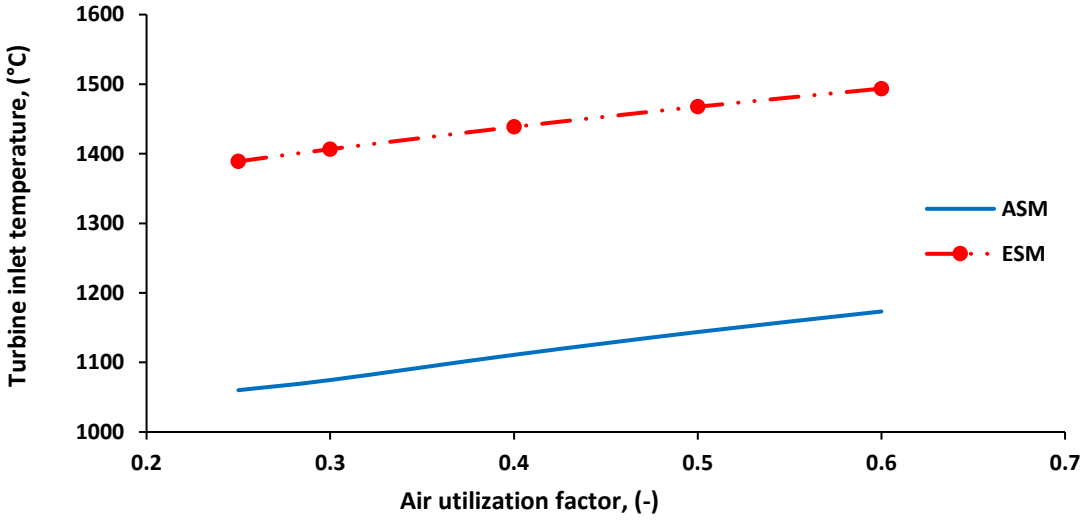

Figure 15. Variation of turbine inlet temperature with air utilization factor for two various models.

The effect of U_a on the net power of the gas turbine for two different models reveals in Figure 16. The gas turbine net power decreases with an increase in the U_a due to the GT power output reduction at higher U_a because of the decrease in the mass flow rate of air to the GT. The increase in the U_a has a positive impact on raising the TIT, but the reduction in the mass flow rate across GT has a more significant effect on decreasing the power of GT. It is also shown that the power produced by the GT for the ESM is much greater than the ASM because the ESM works at high SOFC operating temperature. It is shown from the results that the net power of GT decreases from 102 to 82.3 kW (about 19.3%) for the ASM, whereas it decreases from 237.3 to 148.7 kW (about 37.34%) for the ESM when the U_a increases from 0.25 to 0.6.

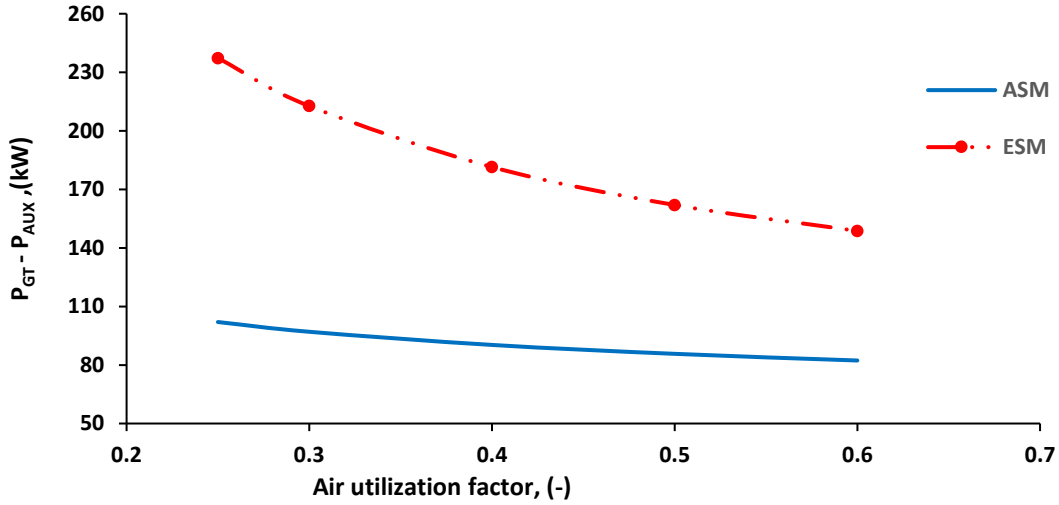

Figure 16. Variation of net power of the gas turbine with air utilization factor for two various models

Figures 17 and 18 show the impact of U_a on the performance of the integrated system for two different models. It is worth indicating that a higher U_a hurts the efficiencies of the overall system. It is shown from the curves that the SOFC efficiencies and overall system efficiencies decrease with increasing the U_a due to the decrease in the SOFC power density and the overall power generated from the integrated system. It is presented from the results that the SOFC efficiency decreases from 56 to 55.1% for the ASM, whereas it reduces from 41.83 to 40.7 % for the ESM. The SOFC exergy drops from 54 to 53.13% for the ASM.

In contrast, it reduces from 40.34 to 39.26% for the ESM. These figures also reveal that the overall system efficiencies still decrease because of a sharp decrease in GT's net power. It is clear from the result that the overall system efficiency reduces from 65.5 to 62.73% for the ASM, whereas it reduces from 63.88 to 54.52% for the ESM.

The overall system exergy decreases from 63.17 to 60.51% for the ASM and reduces from 61.62 to 52.6% for the ESM.

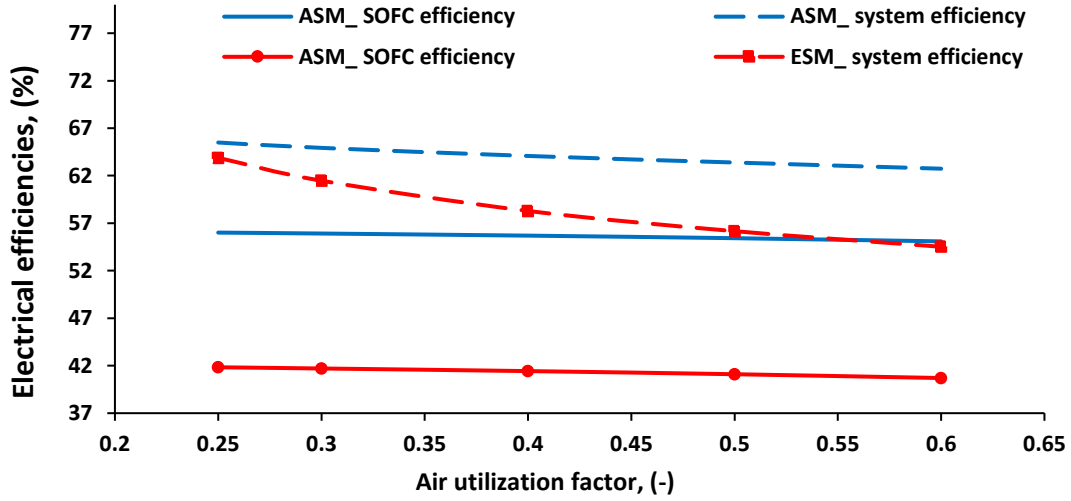

Figure 17. Variation of Electrical efficiencies with air utilization factor for two various models.

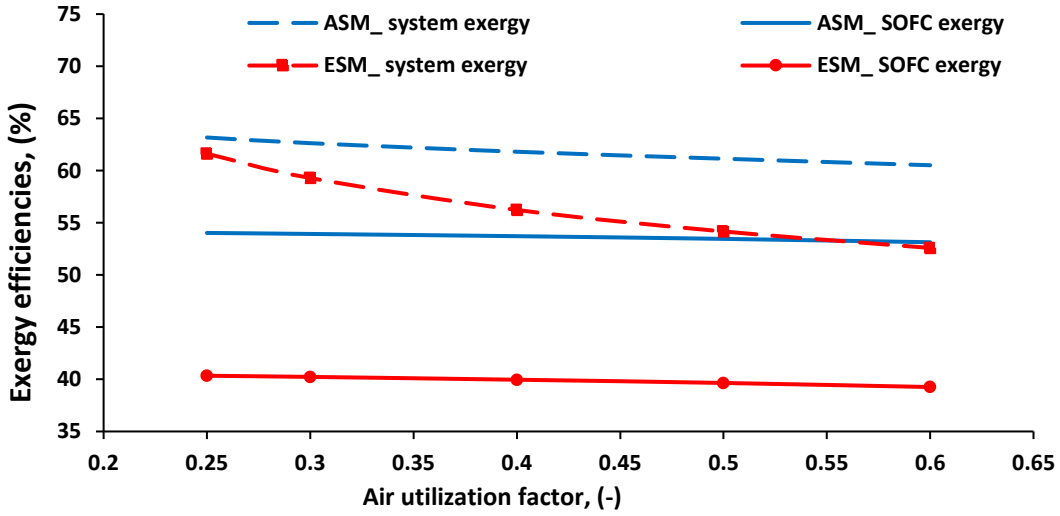

Figure 18. Variation of Exergy efficiencies with air utilization factor for two various models.

Table 5 illustrates the performance-related results of the existing system at optimum points obtained from the simulation. According to Table 4, the power generated from the SOFC and GT for ASM at the optimum condition of the hybrid system is 601kW, 94.4 kW, respectively. In contrast, the power generated from the SOFC and GT for ESM at the hybrid system's optimum condition is446kW, 181.3 kW, respectively. The table also showed that electrical efficiency and exergy at the optimum condition are 64.61% and 62.32% for the ASM, whereas electrical efficiency and exergy are 58.3% and 56.23% for the ESM.

Table 5. Main results of the simulation at optimum points

Parameter	**ASM**	**ESM**
Cell voltage (V)	0.697	0.522
SOFC power (kW)	624.1	450.2
Net electrical power output from GT (kW)	93.7	180.1

Total electrical power output (kW)	717.8	630.3
SOFC electrical efficiency (%)	55.92	41.84
SOFC electrical exergy (%)	53.94	40.32
Electrical efficiency of the hybrid system (%)	64.6	58.58
Electrical exergy of the hybrid system (%)	62.32	56.51

CONCLUSION

The comparison between anode and electrolyte SOFC hybrid integrated with the Brayton cycle led to several unique findings potentially of great benefit to power sector professionals.

1- A considerable increase in the overall power can be noticed, with a maximum of 695 kW at 7.7 bar for the ASM model and a maximum of 630.3 kW at 12 bar for the ESM model, a significant increase 9.31% for the anode-supported model.
2- When utilizing the anode-supported model, the SOFC, and GT, contribute 83.7% and 16.3%, respectively, to the total power output. In contrast, the SOFC and GT contribute 71.1% and 28.9%, respectively, to the total power output with the electrolyte-supported model.
3- The high SOFC operating pressure impulse an increment in the cell voltage, consequently improving the overall power, efficiency, and exergy of SOFC.
4- Increasing the hybrid system's operating pressure causes an increase in overall power and efficiencies until it reaches an upper point and then falls as the operating pressure increases.
5- Reducing the fuel utilization factor positively influences the stack voltage, SOFC power output, and the hybrid system's total power. On the other hand, it negatively affects the electrical efficiencies and exergy efficiencies of the hybrid system.
6- Increasing the fuel utilization factor enhances the hybrid model's performance and diminishes the cost of fuel.
7- Increment the air utilization factor negatively affects the electrical power output and overall system's efficienciesdue to the reduction in the O_2concentration at the cathode-electrolyte interface.

NOMENCLATURE

A_{cell}	Cell area (cm^2)
E°	Fuel cell voltage at standard conditions (V)
$\dot{E}$	Rate of energy (W)
F	Faraday constant (C mol^{-1})
ΔG	Different in Gibbs free energy (J mol^{-1} k^{-1})
i	Current density (A/ cm^2)
h	Enthalpy (J mol^{-1})
LHV	Lower heating value (J. mol^{-1})
$\dot{m}$	Mass flow rate (kg s^{-1})
n_{cell}	Number of cells
P_{el}	Electrical power generated (W)

Greek Letters

δ	Thickness (cm)
H	Polarization, V

H	Efficiency, %
P	Electrical resistivity (Ω^{-1} cm^{-1})
ϵ	Overall heat transfer coefficient
λ	The stoichiometric ratio of air

Superscripts and Subscript

A	Anode
act	Activation
C	Cathode
con	Concentration
e	Electrolyte
f	Fuel
i	Interconnection
in	Inlet
ohm	Ohmic
out	Outlet

Abbreviations

A/F	Air fuel ratio
ASM	Anode-supported model
CC	Combustion chamber
ESM	Electrolyte-supported model
FC	Fuel compressor
GT	Gas turbine
M	Mixer
Rec	Recuperator
S/C	Steam carbon ratio
SOFC	Solid oxide fuel cell
SOFC/GT	Solid oxide fuel cell – gas turbine
ST	Steam turbine
TIT	Turbine inlet temperature
U_a	Air utilization factor
U_f	Fuel utilization factor

REFERENCES

[1] McPhail SJ, Aarva A, Devianto H, Bove R, Moreno A. SOFC and MCFC: Commonalities and opportunities for integrated research. Int. J. Hydrogen Energy, 2011. https://doi.org/10.1016/j.ijhydene.2010.09.071.

[2] Choudhary T, Sanjay. Thermodynamic assessment of advanced SOFC-blade cooled gas turbine hybrid cycle. Int J Hydrogen Energy 2017. https://doi.org/10.1016/j.ijhydene.2017.02.178.

[3] Akroot A, Namli L, Ozcan H. Compared Thermal Modeling of Anode- and Electrolyte-Supported SOFC-Gas Turbine Hybrid Systems. J Electrochem Energy Convers Storage 2021. https://doi.org/10.1115/1.4046185.

[4] Larminie J, Dicks A. Fuel cell systems explained: Second edition. 2013. https://doi.org/10.1002/9781118878330.

[5] Tsai A, Pezzini P, Tucker D, Bryden KM. Multiple-model adaptive control of a hybrid solid oxide fuel cell gas turbine power plant simulator. J Electrochem Energy Convers Storage 2019. https://doi.org/10.1115/1.4042381.

[6] Dumitrescu A, Lee TW, R. P. Roy. Computational Model of a Hybrid Pressurized Solid Oxide Fuel Cell Generator/Gas Turbine Power Plant. J Energy Resour Technol 2011;133.

[7] Oryshchyn D, Harun NF, Tucker D, Bryden KM, Shadle L. Fuel utilization effects on system efficiency in solid oxide fuel cell gas turbine hybrid systems. Appl Energy 2018. https://doi.org/10.1016/j.apenergy.2018.07.004.

[8] Araki T, Ohba T, Takezawa S, Onda K, Sakaki Y. Cycle analysis of planar SOFC power generation with serial connection of low and high temperature SOFCs. J Power Sources 2006. https://doi.org/10.1016/j.jpowsour.2005.09.003.

[9] Singh O, Singh R. Thermodynamic evaluation of SOFC-GT hybrid power and cooling system. Energy Sources, Part A Recover Util Environ Eff 2019;00:1–15. https://doi.org/10.1080/15567036.2019.1663307.

[10] Suther T, Fung AS, M. Koksal, F. Zabihian. Effects of operating and design parameters on the performance of a solid oxide fuel cell–gas turbine system. Int J Energy Res 2011;35:616–32. https://doi.org/10.1002/er.1722.

[11] Pierobon L, Rokni M. Thermodynamic analysis of an integrated gasification solid oxide fuel cell plant with a kalina cycle. Int J Green Energy 2015. https://doi.org/10.1080/15435075.2013.867267.

[12] Huang Y, Turan A. Fuel sensitivity and parametric optimization of SOFC – GT hybrid system operational characteristics. Therm Sci Eng Prog 2019. https://doi.org/10.1016/j.tsep.2019.100407.

[13] Kuchonthara P, Bhattacharya S, Tsutsumi A. Energy recuperation in solid oxide fuel cell (SOFC) and gas turbine (GT) combined system. J Power Sources 2003. https://doi.org/10.1016/S0378-7753(03)00009-0.

[14] Palsson J, Selimovic A, Sjunnesson L. Combined solid oxide fuel cell and gas turbine systems for efficient power and heat generation. J Power Sources 2000. https://doi.org/10.1016/S0378-7753(99)00464-4.

[15] Jia J, Abudula A, Wei L, Shi Y. Performance comparison of three solid oxide fuel cell power systems. Int J Energy Res 2013;37:1821–30. https://doi.org/10.1002/er.3000.

[16] Sarmah P, Gogoi TK. Performance comparison of SOFC integrated combined power systems with three different bottoming steam turbine cycles. Energy Convers Manag 2017. https://doi.org/10.1016/j.enconman.2016.11.009.

[17] Chitsaz A, Hosseinpour J, Assadi M. Effect of recycling on the thermodynamic and thermoeconomic performances of SOFC based on trigeneration systems; A comparative study. Energy 2017. https://doi.org/10.1016/j.energy.2017.02.019.

[18] Sghaier SF, Khir T, Ben Brahim A. Energetic and exergetic parametric study of a SOFC-GT hybrid power plant. Int J Hydrogen Energy 2018. https://doi.org/10.1016/j.ijhydene.2017.08.216.

[19] Saebea D, Authayanun S, Patcharavorachot Y, Arpornwichanop A. Effect of anode-cathode exhaust gas recirculation on energy recuperation in a solid oxide fuel cell-gas turbine hybrid power system. Energy 2016. https://doi.org/10.1016/j.energy.2015.10.138.

[20] Haseli Y, Dincer I, Naterer GF. Thermodynamic modeling of a gas turbine cycle combined with a solid oxide fuel cell. Int J Hydrogen Energy 2008. https://doi.org/10.1016/j.ijhydene.2008.05.036.

[21] Amati V, Sciubba E, Toro C. Exergy analysis of a solid oxide fuel cell-gas turbine hybrid power plant. ASME Int Mech Eng Congr Expo Proc 2009;8:721–31. https://doi.org/10.1115/IMECE2008-68339.

[22] Keshvarparast A, Ajarostaghi SSM, Delavar MA. Thermodynamic analysis the performance of hybrid solar-geothermal power plant equipped with air-cooled condenser. Appl Therm Eng 2020. https://doi.org/10.1016/j.applthermaleng.2020.115160.

[23] Ezoji H, Mousavi SS, Ajarostaghi. Compression ignition (HCCI) engine by Recuperative organic Rankine Cycle (RORC): Effect of operational parameters. Energy 2020;205. https://doi.org/10.1016/j.energy.2020.117989.

[24] Abbasi H, Rahimpour F, Rahimpour F, Kasaeian A. Evaluating integration of biomass gasification process with solid oxide fuel cell and torrefaction process. J Therm Eng 2019;5:230–9. https://doi.org/10.18186/thermal.654637.

[25] Ranjbar F, Chitsaz A, Mahmoudi SMS, Khalilarya S, Rosen MA. Energy and exergy assessments of a novel trigeneration system based on a solid oxide fuel cell. Energy Convers Manag 2014. https://doi.org/10.1016/j.enconman.2014.07.014.

[26] Mehr AS, Mahmoudi SMS, Yari M, Chitsaz A. Thermodynamic and exergoeconomic analysis of biogas fed solid oxide fuel cell power plants emphasizing on anode and cathode recycling: A comparative study. Energy Convers Manag 2015. https://doi.org/10.1016/j.enconman.2015.07.085.

[27] Akroot A, Ekici Ö, Köksal M. Process modeling of an automotive pem fuel cell system. Int J Green Energy 2019. https://doi.org/10.1080/15435075.2019.1641105.

[28] Ozcan H, Dincer I. Performance evaluation of an SOFC based trigeneration system using various gaseous fuels from biomass gasification. Int J Hydrogen Energy 2015;40:7798–807. https://doi.org/10.1016/j.ijhydene.2014.11.109.